Sensitivity of post-tensioned concrete wall response to modelling of damping

J. O'Hagan, K.M. Twigden, Q.T. Ma

The University of Auckland, Auckland, New Zealand.

2013 NZSEE Conference

ABSTRACT: Post-tensioned rocking concrete wall systems are effective, low-damage structural solutions for seismic regions. This paper presents an experimental and numerical investigation which aimed to provide guidance to the designer in selecting a damping mechanism and magnitude of damping ratio for numerical modelling of these systems. The study examined the effectiveness of Coulomb friction, coefficient of restitution (COR) and equivalent viscous damping (EVD) models for simulating their response to snap back tests and earthquake motion. It is shown that no model alone is able to reproduce the required amplitude decay and maintain phase. However a friction model combined with either COR or EVD approach provided accurate results. Pseudo-dynamic (PSD) earthquake simulations for different optimised combinations illustrated that a model that is effective in modelling free vibration response may not work well for earthquake simulation due to history dependency and damping sensitivity. Post-tensioned rocking concrete walls with added hysteretic dampers provided results that are much less sensitive to numerical damping choices. The combination of friction and COR models is recommended for analyses.

1 INTRODUCTION

The current design philosophy seeks low damage structural solutions that minimise both repair cost and occupancy down time following a seismic event. One such system is the unbonded post-tensioned precast concrete wall which is permitted to rock at its base. Base uplift due to rocking eliminates the development of concrete tensile stresses at the wall base and provides a pseudo "base isolation effect" through the elongation of the system's structural period. This system is characterised by a softening force displacement response with minimal damage as a result of geometric nonlinearity. The lack of damage or hysteresis suggests these systems have limited energy dissipation compared to an equivalent traditionally reinforced concrete structure.

Under dynamic disturbance, a single unbonded post-tensioned concrete wall dissipates energy through contact damping from impacts during rocking motion, friction damping at the unbonded interfaces and inherent material damping. Despite this simple and logical separation, the overall energy dissipation is often difficult to disaggregate into these components, and there is not a universally accepted technique for modelling contact damping (Ma 2010).

This paper presents an investigation into the dynamic response of a single unbonded post-tensioned precast concrete wall, or a Single Rocking Wall (SRW). This study attempts to emulate the displacement history of a series of snap-back experiments using various damping representations through a single degree of freedom (SDOF) numerical model.

2 THE SRW SYSTEM

The data set for this study included a series of pseudo-static and dynamic snapback tests performed on four SRWs (Twigden et al. 2012). The wall specimens were 3 m high, 1 m wide and 0.12 m thick. The walls had specifically designed confinement reinforcement at the toe regions and additional armouring by way of two 25 x 25 x 5 steel equal angles at the wall corners. Each wall had two 15 mm diameter tendons stressed to 0.27 times the yield stress (f_y). The tendons had a yield stress of 900 MPa and

ultimate strength (f_u) of 1100 MPa. The precast concrete wall panels had a compressive strength of 35 MPa. The SRW sat on a foundation and a 1237 kg concrete block was attached to the top of the wall to provide mass, tendon anchorage and to act as a loading beam. An actuator was attached to the loading beam, 3.1 m above the wall base. An additional 812 kg mass was attached above the loading beam. A photo of this setup is presented in Figure 1. Further information about the experimental test is available a companion paper by Twigden et al. (2013).

Figure 1 The SRW setup for testing

2.1 **Force-displacement performance**

The experimental force displacement response of the SRW system is presented in Figure 2a. Notable features are the reduction in stiffness above 0.25 % drift and the minimal hysteretic energy dissipation. Figure 2b presents a numerical simulation of the experimental response. The numerical model, which is also used in subsequent analyses, consists of a nonlinear elastic restoring element and a 0.5 kN friction element in parallel.

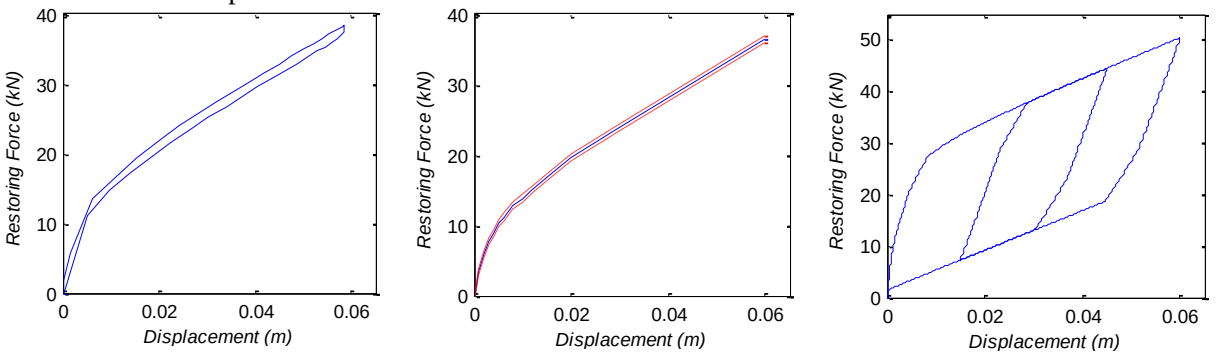

Figure 2 Force-displacement response - a) experimental SRW; b) numerical SRW approximation; and c) numerical SRW with mild steel hysteretic dampers

3 **DYNAMIC RESPONSE AND DAMPING**

Damping is defined as the reduction in amplitude of a vibratory oscillation as a result of energy being removed from the system by the work done through frictional forces. Friction in a vibrating structural system can be classified as material, boundary and fluid damping (de Silva 2008).

3.1 **Damping mechanisms**

Material or inherent damping refers to energy dissipated due to macroscopic and microscopic processes within the material (de Silva 2008). A common example of material damping is the visco-elastic material model in which the material damping is assumed to be viscous. Hysteretic damping is another form of inherent damping which by definition is frequency independent. Hysteretic damping encapsulates inelastic behaviour where material yielding dissipates energy. Boundary damping encompasses the dissipation that occurs at the interfaces between structural members. Boundary damping manifests as a result of relative motions between components, such as friction between sliding surfaces or impacts between unbonded surfaces. Fluid damping occurs when a structure interacts with a surrounding fluid, typically air. The drag forces induced in the fluid cause energy to be dissipated in a viscous manner. Civil engineering structures will generally exhibit all three mechanisms at varied magnitudes of dissipation and spatial distributions.

3.2 **Damping in analysis**

In linear numerical analyses, it is typical to represent all energy dissipation through equivalent viscous damping irrespective of the damping mechanism sources. The justification is that damping forces are typically an order of magnitude smaller than the concurrent inertial and restoring forces, so an equivalent amount of energy dissipated over an entire oscillation is representative of the instantaneous mechanisms throughout (Chopra 2007). This simplification also assists the dynamic solution process in that linear viscous damping, as it enables the disaggregation of a multi degree of freedom (MDOF) problem into a set of SDOF modal coordinates (Wilson and Penzien 1972). With a single viscous damping term, the governing equation of dynamic motion for free vibration of a linear system is:

$$M\ddot{u} + C\dot{u} + f_s = 0 \tag{1}$$

where M is the mass matrix, C the viscous damping matrix, f_s the stiffness force vector, and $\dot{u}$ and $\ddot{u}$ the velocity and acceleration vectors at the nominated degrees of freedom (DOFs) respectively. In a linear elastic system, the stiffness force $f_s = Ku$, where K is the stiffness matrix and u the displacement vector. For linear MDOF systems, assuming classical damping, in other words the distribution of viscous damping forces is proportional to the distribution of inertial and restoring forces, Equation 1 can be rewritten as a set of uncoupled differential equations in the modal coordinates, y. This is presented as Equation 2 below.

$$m\ddot{y} + c\dot{y} + ky = \ddot{y} + 2\xi\omega\dot{y} + \omega^2 y = 0 \tag{2}$$

The viscous damping coefficient for each modal coordinate is specified as $c = 2\xi\omega m = 2\xi k/\omega$, where ξ is the fraction of critical viscous damping, ω the natural frequency of the mode of interest, m the modal mass, and k the modal stiffness. The equation for c reveals that this technique in specifying viscous damping is proportional to the structures vibratory properties.

When a system has nonlinear stiffness properties the equivalent viscous damping approach becomes more difficult to justify. The stiffness force vector becomes some nonlinear function $f_s = f(u, \dot{u})$ so it is difficult to justify which structural dynamic properties to use in the damping coefficient formulation, as in the analysis of SDOF SRWs.

3.3 **SRW dynamic snapback response**

The SRW described in Section 2 was pulled back to the design drift level of 2%, or 60 mm, and released to vibrate freely. The test was then replicated using the pseudo-dynamic (PSD) testing method, 1) without any numerically modelled damping, and 2) with 1.2 % initial secant stiffness proportional damping as recommended by Marriott (2009). The displacement time histories are presented in Figure 3 below. The undamped PSD response encapsulates all non-dynamic damping effects and is significantly under-damped, which indicates rate dependent (dynamic) damping mechanisms must be accounted for. The 1.2 % EVD is shown to provide too much dissipation.

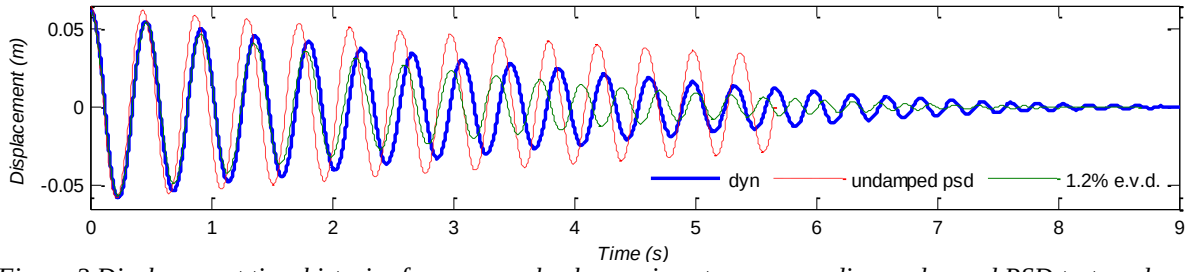

Figure 3 Displacement time histories from a snap back experiment, corresponding undamped PSD test, and corresponding PSD test with 1.2 % initial secant stiffness proportional EVD

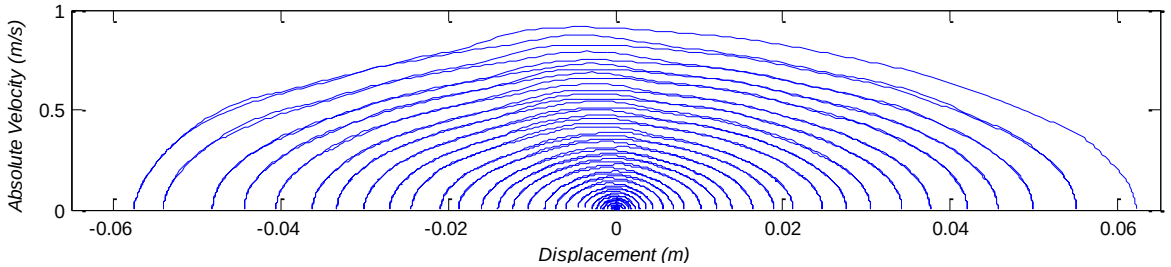

Figure 4 Phase plot for the dynamic snapback test

Inspection of the phase plot in Figure 4 reveals a significant reduction in velocity following the crossing of the zero displacement position. This can be attributed to the boundary damping associated with the impact against the foundation as the wall rocks from one corner to the other. It is essential to account for this rate dependent dissipation in analysis to achieve accurate time history response.

3.4 **Damping models**

This study used two approaches to simulate the boundary damping of the SRW system, i) using a coefficient of restitution model to simulate the effect explicitly, and ii) by adopting equivalent viscous damping to model the overall effect.

3.4.1 *Coefficient of restitution*

Housner (1963) quantified the reduction in angular velocity of a rocking object that passes through an impact using the coefficient of restitution, r, as defined by

$$r = \left(\frac{\dot{\theta}_2}{\dot{\theta}_1}\right)^2 = \left(\frac{\dot{u}_2}{\dot{u}_1}\right)^2 \tag{3}$$

where $\dot{\theta}$ is the angular velocity, $\dot{u}$ the translational velocity at the top of the wall, and subscripts 1 and 2 denote the entry and exit values respectively. Figure 5 shows a number of numerically simulated time histories for the wall. The analyses utilised the nonlinear force displacement response outlined earlier including the 0.5 kN Coulomb friction component and a varying coefficient of restitution.

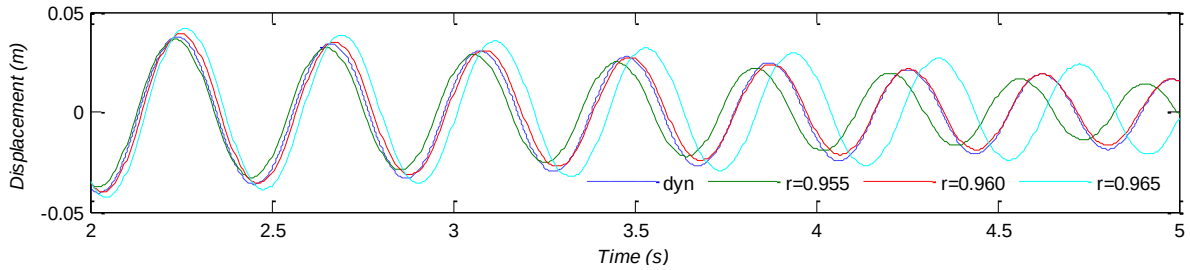

Figure 5 Numerical displacement time histories implementing damping via constant Coulomb friction and COR

Figure 5 highlights that this combination of damping models can accurately reproduce both the amplitude and phase of response. A r value of 0.96 produced the best matching with the experimental data and this corresponds to a velocity reduction of 0.9798 following impact. Previous research by Ma

(2010) regarding post tensioned masonry walls concluded a single value of r alone could not emulate the dynamic response of the entire amplitude range. In this case, if friction is modelled separately the coefficient of restitution is an accurate model for damping in the system.

3.4.2 *Equivalent viscous damping (EVD)*

The alternative to directly quantifying the energy dissipation associated with impacts is to adopt an equivalent amount of viscous damping. The SDOF damping coefficient must be carefully selected with consideration of the SRW's nonlinear stiffness. Figure 6 presents the four different stiffness proportional damping that are considered in this study, i) initial tangent stiffness (K_{ti}) proportional, ii) target secant stiffness (K_{si}) proportional with the target being the initial displacement for the snapback test, iii) updated secant stiffness (K_s) proportional, and iv) updated tangent stiffness (K_t) proportional. The first two initial proportional schemes reduce to the same mathematical problem, as they each converge to a constant damping coefficient. The updated schemes are history dependent.

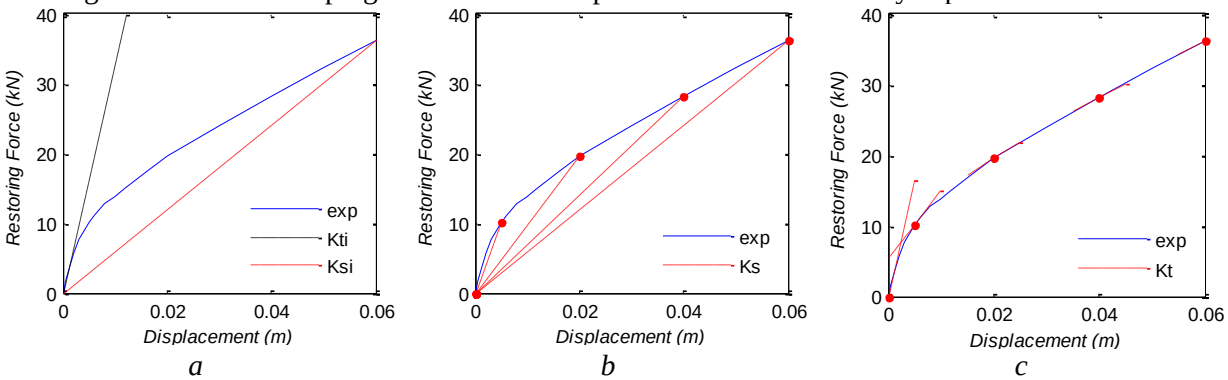

Figure 6 The four stiffness schemes – a) initial tangent andsecant, b) updated secant, and c) updated tangent

3.4.3 *Friction*

The effect of friction can be directly modelled in the equation of motion or indirectly through equivalent viscous damping. Numerical simulation results using the initial stiffness proportional equivalent viscous damping approach, shown in Figure 6, illustrate that a single EVD coefficient alone cannot match the phase and amplitude of the experimental data across the entire time range. This highlights that importance of modelling friction explicitly.

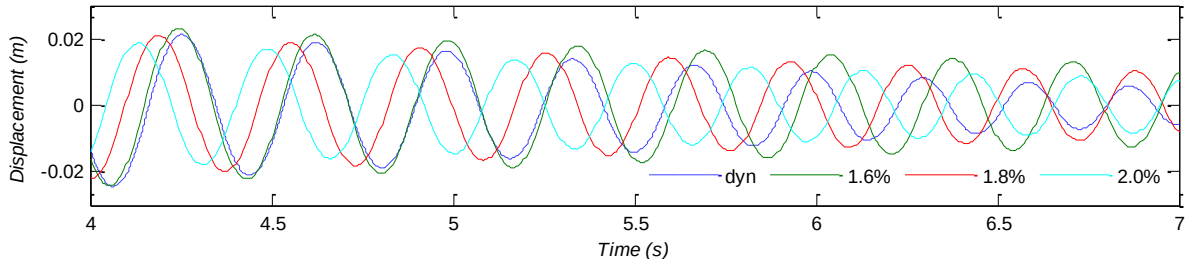

Figure 7 Numerical displacement time histories implementing initial tangent stiffness proportional EVD only

3.5 **Analysis procedure**

Numerical analyses presented in this paper represent the SRW as a single translational DOF located at the top of the wall. The equation of motion is defined as,

$$M\ddot{u} + C\dot{u} + f_s \pm F_{fr} = 0 \qquad (4)$$

where f_s is the nonlinear elastic backbone curve derived from the quasi-static experiment, F_{fr} is a constant 0.5 kN Coulomb friction force that opposes the direction of motion (magnitude of which was determined from the half height of the hysteresis opening), and all other terms as previously stated.

The governing equation is solved using the Newmark Explicit Method (NEM) numerical integration scheme with a time step size of 0.005 s. A constant damping coefficient is selected once only at the

start of the solution process for the single stiffness proportional schemes. The updated tangent stiffness scheme derives a new tangent stiffness value on every time step iteration from the stiffness across the current time step n expressed mathematically as,

$$K_{t,n} = \left|\frac{f_{s,n+1} - f_{s,n}}{u_{n+1} - u_n}\right| \tag{5}$$

The explicit integrator allows the tangent stiffness to be calculated using forward difference. The updated secant stiffness recalculates the stiffness value on every iteration based on the deformation state at the end of the current time step. This is expressed mathematically as,

$$K_{s,n} = \left|\frac{f_{s,n+1}}{u_{n+1}}\right| \tag{6}$$

4 NUMERICAL SENSITIVITY TO EVD DAMPING CHOICES

A series of time history analyses were conducted to assess the ability of each equivalent viscous damping formulation to emulate the experimental response. The equivalent viscous damping ratio, ξ, was varied by 0.001 increments for each formulation. A graphical example of the procedure is presented in Figure 8 for the updated tangent stiffness case. Figure 8 demonstrates that a combination of friction and viscous damping can emulate the dynamic peaks and maintain both phase and amplitude over the entire range of motion. It is also evident that the accuracy of the analysis is extremely sensitive to the chosen damping ratio due to the history dependency of the problem.

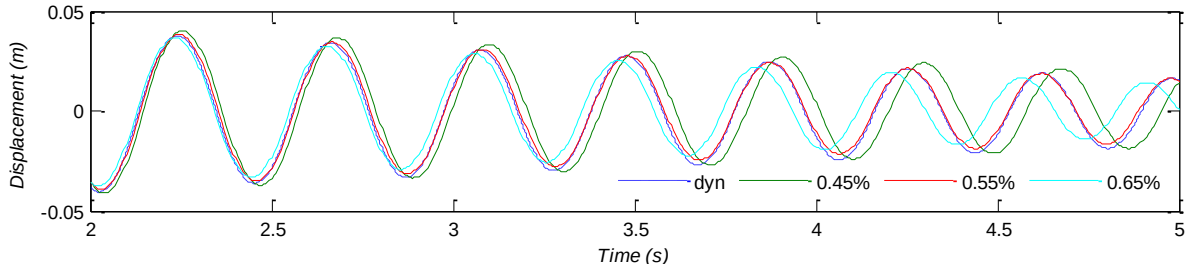

Figure 8 Numerical displacement time histories for analyses adopting updating tangent stiffness proportional EVD and friction compared to the actual dynamic response

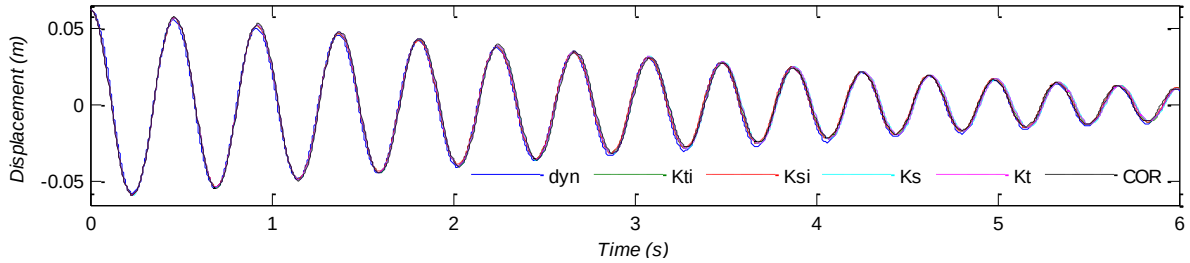

Figure 9 Best fit numerical displacement time histories for the five damping schemes compared to the actual dynamic response

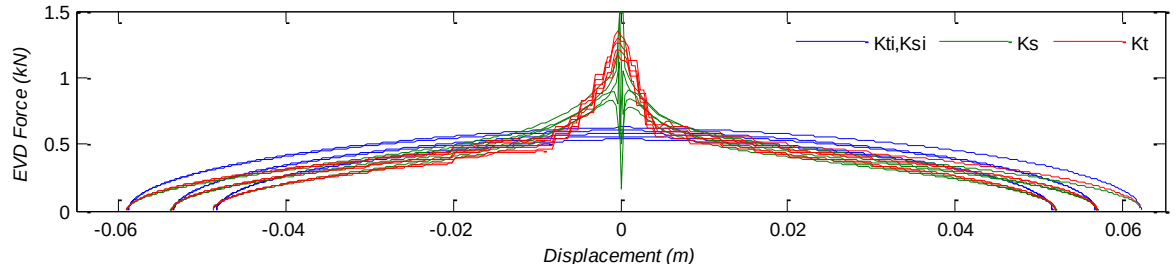

Figure 10 EVD force as a function of displacement for the four optimised damping schemes over the first three oscillations (others omitted for clarity)

The four sets of analyses reveal that all of the EVD schemes can accurately model the experimental results. This is evident from the four indistinguishable optimal responses presented in Figure 9. Figure

10 presents the damping force, $f_d = C\dot{u}$, with respect to displacement. Figure 10 also highlights that the two updated schemes have increasing damping forces approaching the zero displacement (the upright position) where the stiffness increases. This aligns well with the reality of impact damping where more energy is dissipated close to zero displacement.

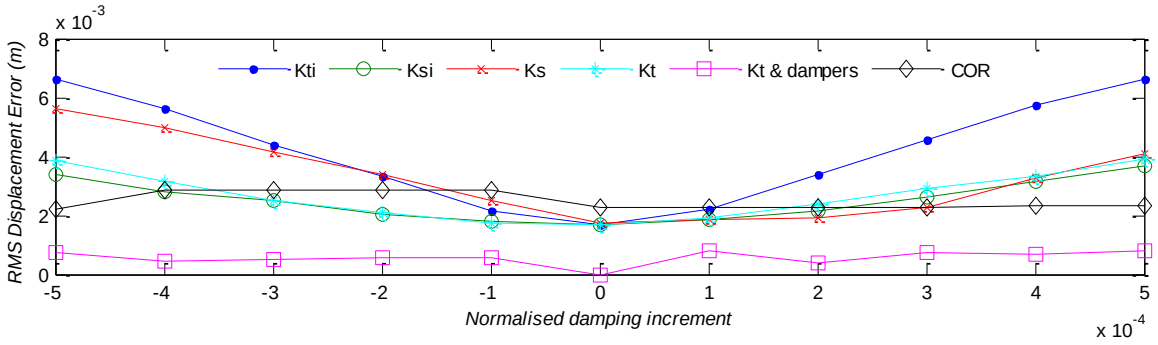

Figure 11 Root mean square of displacement error with respect to variation in damping ratio away from optimal value

The relative sensitivity of the four schemes to change in EVD ratio was evaluated by comparing the Root Mean Square (RMS) of the displacement errors in the time history. Figure 11 plots the RMS error as a function of the damping ratio. The x ordinates were normalised by the optimal value to reveal the effect of changing the EVD ratio either side of the best fitting value. The Figure shows that the initial tangent stiffness scheme is the most sensitive scheme, which is not surprising as this scheme uses the largest stiffness value to generate the damping ratio. Both the updated tangent stiffness and the initial secant stiffness schemes appear to be the least sensitive to changes in EVD ratio. Considering the nature of the damping forces and the reduced sensitivity to a selected damping ratio, it is determined that the two updated coefficient schemes are the most suitable for analysis of SRWs. In comparison, the RMS error for the COR model is less sensitive to the same small increments in r, but does not reach the same minimum error value.

5 VERIFICATION WITH PSEUDO DYNAMIC TESTING

As a further verification, the two updated coefficient schemes were implemented in PSD snapback tests of the same SRW. The PSD test method shared the same solution process as the numerical simulations with the exception that the restoring forces ($f_s + F_{fr}$) were experimentally measured. Figure 12 presents the displacement time histories, and Table 1 summarises the damping ratios. The first round of tests using the optimised numerically determined damping ratios in section 4 showed that there was too much energy dissipation in the system. It is postulated that the real friction forces are larger than the simple constant value in the numerical analyses, thus the damping ratios optimised previously are too high. The tests were repeated with revised with lower damping ratios and this lead to more accurate simulations as shown in Figure 13.

Table 1 Damping ratios used in the presented analyses and tests

Damping Type	Optimal damping Ratio from Numerical analysis	Revised Ratios for PSD Snap Back Tests	Revised Ratios for PSD Tests with Earthquake Inputs
K_{ti}	0.00325		
K_{si}	0.00775		
K_s	0.00525	0.00350	0.00425
K_t	0.00700	0.00400	0.00550

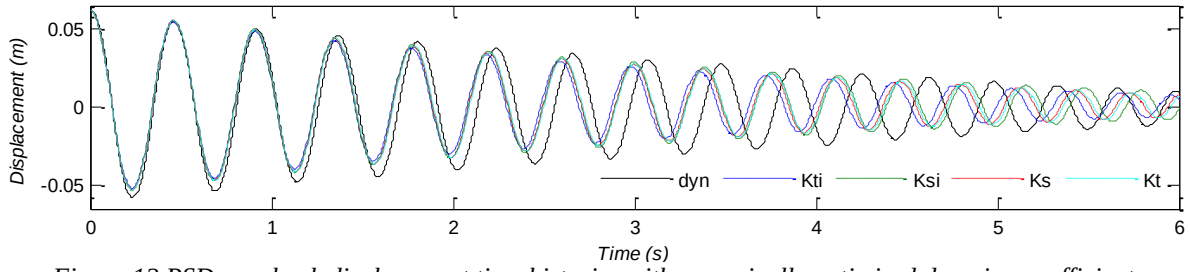

Figure 12 PSD snapback displacement time histories with numerically optimised damping coefficients

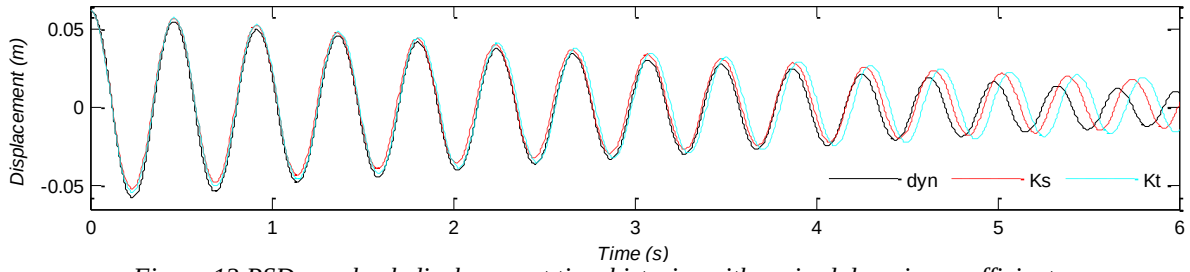

Figure 13 PSD snapback displacement time histories with revised damping coefficients

The PSD test method was then used to subject the SRW to earthquake ground motion from the February 22nd 2011 Lyttleton earthquake. The earthquake record selected for the tests was the East-West motion recorded at the Resthaven (REHS) site. The acceleration amplitude was increased 1.25 times to achieve a target drift of 2% or 60 mm. Figure 14 plots the resulting displacement time histories from the two PSD tests with updating secant and tangential stiffness EVD. The plot shows significant divergence of the two tests as the simulation progressed. This divergence highlights the sensitivity of SRWs to damping mechanism choices, and suggests that earthquake performance of rocking walls cannot be inferred from free vibration tests alone.

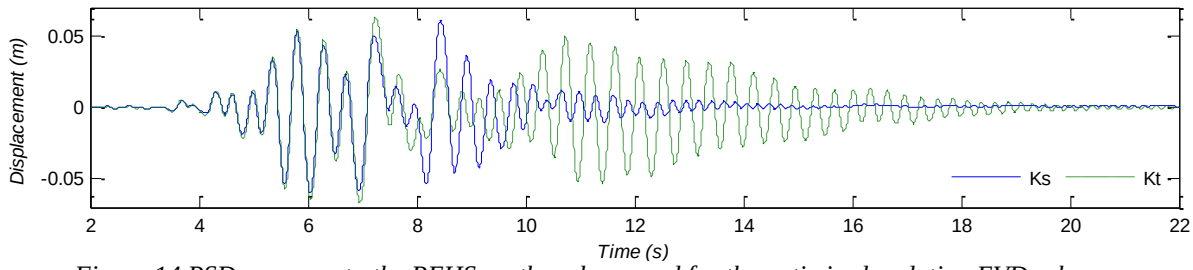

Figure 14 PSD response to the REHS earthquake record for the optimised updating EVD schemes

6 EFFECT OF ADDED DAMPING DEVICES

Post tensioned rocking walls are often supplemented with additional damping devices to help dissipate energy in seismic events. The presented analyses and tests have shown SRWs to be extremely sensitive to small changes in EVD ratio, but research has suggested that the added dissipation is much larger than the inherent damping and hence the sensitivity to EVD ratio is inconsequential (Marriott 2009). A numerical analysis was conducted on the same SRW with partially debonded yielding mild steel bars placed across the rocking interface, adjacent to the location of the unbonded post tensioning as an added damping measure. One 12 mm bar was placed either side of the centreline to give a moment capacity increase of 25 % at design drift. The steel bars were modelled as elasto-plastic elements with a yield stress of 300 MPa. This gave rise to a simulated hysteresis as shown in Figure 2c. The new response shows significantly more energy dissipated hysteretically through the flag-shaped behaviour, amounting to an EVD ratio proportional to the initial tangent stiffness of 0.0254 over one oscillation at design drift, or 7.8 times greater than that calculated for the SRW alone.

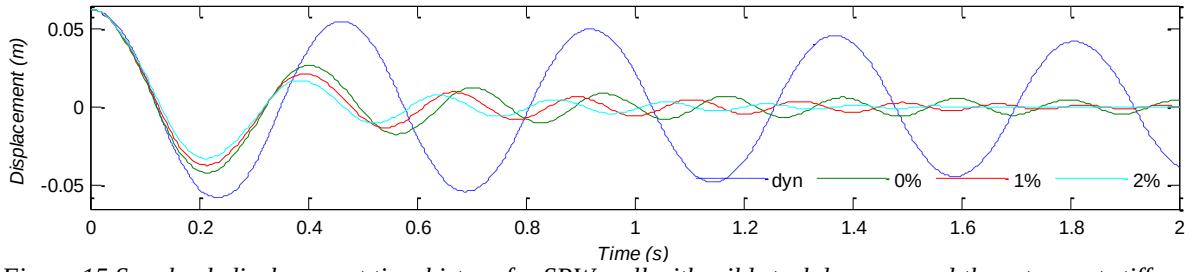

Figure 15 Snapback displacement time history for SRW wall with mild steel dampers and three tangent stiffness proportional EVD analyses compared to dynamic SRW response

The response of the wall with hysteretic dampers in Figure 15 exhibited much faster amplitude decay than the wall alone. The sensitivity to damping ratio for simulating free vibration response is shown to be much less significant than the corresponding results in Figure 11 for the SRW alone. The numerical responses in Figure 15 have damping ratios varied in 0.5 % increments from 0-2 % that are more realistic of typical engineering analyses. Figure 15 shows that although sensitivity is improved by hysteretic damping, the choice of damping ratio still has considerable effect on both amplitude and phase. Further work is required to confirm the insensitivity hypothesis to earthquake inputs.

7 CONCLUSIONS

This research has shown that the accurate numerical simulation of SRW under free vibration response is extremely sensitive to the selection of numerical damping scheme. COR and EVD models are unable to accurately encapsulate dynamic response unless they are coupled with Coulomb friction. The two updated stiffness proportional EVD damping schemes are the least sensitive to changes in damping ratio and correlate best to the physical mechanisms. A damping ratio of approximately 0.5 % is suitable, one tenth of that typically recommended in structural analysis. The authors recommend the use of the COR as it directly accounts for the impact damping in rocking motion, is less sensitive than EVD, and avoids the choice of which proportional EVD scheme to adopt. Free vibration snapback response alone cannot be used to infer numerical models' performance in simulating SRW response under earthquake excitation. Further experimental testing is required for the validation of the different damping models choice for simulating ground motion input. SRWs with added hysteretic dampers are less sensitive to numerical damping choices, but time history results are still significantly affected by the choice of damping model and EVD ratio.

REFERENCES:

Chopra, A. K. (2007). Dynamics of structures: theory and applications to earthquake engineering. Upper Saddle River, NJ, Prentice Hall.

Silva, C. W. d. (2007). Vibration Damping. Vibration Damping, Control, and Design, CRC Press**:** 1-31.

Housner, G. W. (1963). The behavior of inverted pendulum structures during earthquakes. *Bulletin of the Seismological Society of America* Vol. **53** No. 2: 403-417

Ma, Q. T. M., (2010) The mechanics of rocking structures subjected to ground motion. *PhD--Civil and Environmental Engineering*, University of Auckland. http://hdl.handle.net/2292/5861

Marriott, D., (2009) The Development of High-Performance Post-Tensioned Rocking Systems for the Seismic Design of Structures. Civil Engineering, University of Canterbury Christchurch.

Twigden, K. M., Henry, R. S. and Ma, Q. T. (2012). Dynamic testing of post-tensioned rocking walls. 15th World Conference on Earthquake Engineering, Lisbon, Portugal, 24-28 September

Wilson, E. L. and J. Penzien (1972). "Evaluation of orthogonal damping matrices." International Journal for Numerical Methods in Engineering **4**(1): 5-10.